Two-Dimensional Electron Gases at Complex Oxide Interfaces

Susanne Stemmer[1] and S. James Allen[2]

[1]Materials Department, University of California, Santa Barbara, California 93106-5050; email: stemmer@mrl.ucsb.edu

[2]Department of Physics, University of California, Santa Barbara, California 93106-9530; email: allen@itst.ucsb.edu

Annu. Rev. Mater. Res. 2014. 44:151–71

First published online as a Review in Advance on January 29, 2014

The *Annual Review of Materials Research* is online at matsci.annualreviews.org

This article's doi: 10.1146/annurev-matsci-070813-113552

Keywords

two-dimensional electron gases, 2DEG, $SrTiO_3$, oxide interfaces, perovskites

Abstract

Two-dimensional electron gases (2DEGs) at oxide interfaces may exhibit unique properties, including effects from strong electron correlations, extremely high electron densities, magnetism, and 2D superconductivity. This article discusses routes to high-mobility 2DEGs in complex oxide heterostructures, with a particular focus on 2DEGs that involve transport in $SrTiO_3$. We discuss what is known about the electronic states in $SrTiO_3$ 2DEGs, both experimentally and theoretically. Examples from the current literature are summarized.

1. INTRODUCTION

Oxide heterostructures allow for external control of properties through the manipulation of carrier concentration by composition, electrostatic or modulation doping, and field effect. Furthermore, entirely new phenomena may be caused by two-dimensionality and quantum confinement. These basic concepts have many analogies to conventional semiconductor heterostructures, but the distinctly different electronic structure of oxides requires fundamentally different approaches to both characterization and theoretical description. For example, III–V semiconductor heterostructures, with their wide bands, use states near the bottom of the conduction band that can be described extremely well by an effective mass approximation. In contrast, quantum-confined states in many oxides involve carriers in narrow *d*-bands, which are often substantially filled, and are subject to strong electron-electron correlation effects and exchange coupling, which then dominate the transport properties.

In conventional III–V and group-IV semiconductors, high-quality heterostructures grown by molecular beam epitaxy (MBE) have led to many scientific discoveries, such as the fractional quantum Hall effect (1). The same arguments apply for oxide heterostructures: Only high-quality materials allow the properties of the electron (or hole) system to be governed by intrinsic interactions, such as electron-electron interactions (correlations) or interactions with the lattice, rather than being scattered or trapped by impurities or other defects.

In conventional semiconductor heterostructures, carrier mobility has long been used as a highly sensitive measure of materials and heterostructure quality (2). In particular, at low temperatures, scattering from various imperfections—such as ionized donors or acceptors, impurities, dislocations, interface roughness, alloy disorder, and other defects—limits the mobility (3, 4). Before discussing mobility in oxides, we need to distinguish between the vastly different kinds of classes of oxides. For example, many binary semiconducting oxides, such as ZnO, Ga_2O_3, In_2O_3, and SnO_2, exhibit similarities with conventional semiconductors, such as wide bands and low effective masses. These oxides can exhibit very high mobilities. For example, both the quantum Hall effect and the fractional quantum Hall effect have been observed in $ZnO/Mg_xZn_{1-x}O$ heterostructures (5, 6). Another important class contains the transition metal oxides, which have electronic structures that depend on the degree filling of the *d*-electron states. Oxides with the d^0 electron configuration include binary oxides such as TiO_2 and many perovskite oxides such as $SrTiO_3$ and $KTaO_3$. These oxides have many similarities to the semiconducting oxides, such as relatively low effective masses (on the order of one to a few times m_e, the free electron mass). They have large band gaps and can be described largely by using conventional band models. However, phonon scattering and coupling to the lattice are relatively strong, causing polaron formation, which leads to an enhancement of the effective mass compared with the bare band mass (7). Room temperature mobilities of such oxides are typically much lower than those of conventional semiconductors (8). Magnetic insulating oxides and metallic oxides differ greatly in their electronic structure and properties compared with conventional semiconductors and simple metals, respectively (9). Oxides such as NiO and $YTiO_3$ are Mott insulators (10). They have partially filled *d*-bands, so a metal would be expected according to simple band theory. As is the case for the metallic oxides, electron-electron correlations and coupling to the lattice are very strong. Transitions to various magnetically ordered or charge-ordered phases, and metallic or insulating states, often occur with varying temperature, alloying, magnetic field, or pressure (9, 11). The carrier mobilities in these classes of oxides are generally very low, and transport in these materials is not a subject of this article. Heterostructures involving correlated oxides are discussed by some of the other articles in this volume (12, 13).

This article focuses on high-mobility complex oxide heterostructures that involve at least one d^0 oxide in which transport occurs. To date, most experimental and theoretical studies of such

heterostructures involve conduction in $SrTiO_3$, and we focus mostly on this oxide. In particular, we discuss aspects of electron transport in two-dimensional electron gases (2DEGs) in $SrTiO_3$. Many reviews have already covered interfaces between $LaAlO_3$ and $SrTiO_3$ (14–17). This article takes a more inclusive view of the routes to 2DEGs in $SrTiO_3$, which are discussed in Section 2. We do not discuss emergent phenomena such as magnetism and superconductivity, and we refer readers to the article by Levy and coauthors (13) in this volume.

Compared with the case for conventional semiconductor heterostructures, the development of high-mobility perovskite oxide heterostructures is in its infancy. Epitaxial heterostructures with high crystalline perfection and low extended defect concentrations are state of the art (18, 19), and their growth is facilitated by a wide range of high-quality, single-crystal perovskite substrates with closely matched lattice parameters. Precise control of stoichiometry and reduction of point defect concentrations remain, however, major issues that pose significant challenges in many materials systems. Many studies of $SrTiO_3$ 2DEGs still use a single-crystal substrate, rather than an epitaxial film, as the electrically active side of the interface. We discuss these issues in Section 3. In Section 4, we discuss what is known about the properties of 2DEGs in $SrTiO_3$, and in Section 5, we provide suggestions for future developments.

2. ROUTES TO HIGH-MOBILITY OXIDE HETEROSTRUCTURES

An important prerequisite for a high-mobility 2DEG [or a 2D hole gas (2DHG)] is to minimize scattering from ionized impurities, which dominate the mobility at low temperatures [at room temperature, the mobility of the oxides that are the focus of this article is limited by phonon scattering (8)]. There are two main routes to high-mobility electron (or hole) gases. The first one, invented in 1978, is known as modulation doping (20). Its realization in oxide heterostructures is discussed in Section 2.1. The second approach, to not use any dopants, relies on discontinuities either in the bulk polarization or in the polarity of the surfaces that compose the interface. We discuss these approaches in Section 2.2.

2.1. Modulation Doping

Modulation doping spatially separates conduction electrons (holes) from their donor (acceptor) impurity ion (20). This separation can be achieved, for example, by introducing the latter into a wider-band-gap material, which has a type I (straddling) band-gap alignment with a narrower-band-gap semiconductor, as illustrated in **Figure 1**. This configuration causes the electrons (holes) to be transferred into the narrow-band-gap semiconductor. They remain attracted to donors (acceptors) and create a 2DEG (or 2DHG) at the interface. Scattering due to the ionized donors (acceptors) is dramatically reduced, due to the spatial separation between them and the mobile electrons (holes); such separation is usually further enhanced by adding an undoped spacer layer. The highest-mobility 2DEGs are created by this method, with mobilities exceeding 3×10^7 cm^2 V^{-1} s^{-1} in AlGaAs/GaAs heterostructures (21, 22). Furthermore, this method forms the basis for many important devices, such as high-electron-mobility transistors (HEMTs) (23, 24).

In comparison to the case for conventional semiconductor 2DEGs, modulation doping remains underexplored as a route to 2DEGs in high-mobility complex oxides. We briefly discuss the materials requirements that would allow for modulation doping of, say, a $SrTiO_3$ channel to produce a 2DEG [hole gases in this material are substantially more difficult to produce, due to the inherent doping asymmetry typical of many oxides (25)]. $SrTiO_3$ has a band gap of ~3.2 eV (26). Many wider-band-gap perovskite oxides exist (27, 28) and could be grown epitaxially on $SrTiO_3$. Although data on the band alignments are relatively rare, it is known that, for example, $LaAlO_3$

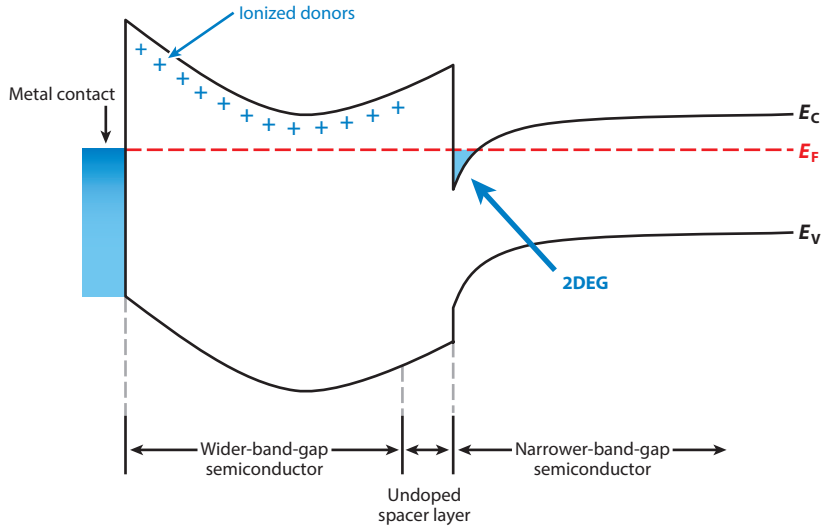

Figure 1

Principle of modulation doping to obtain a high-mobility two-dimensional electron gas (2DEG) (20). Electrons from the donors in the material with the higher-conduction band edge transfer into the conduction band of the semiconductor on the other side of the interface, creating a 2DEG. The electrons are spatially separated from their donors, and ionized impurity scattering is thus reduced. E_C and E_V denote the conduction band edge and valence band edge, respectively, and E_F denotes the Fermi level.

and $SrZrO_3$, which have band gaps of ~5.6 eV (27, 29), have conduction band minima that lie above the conduction band minimum of $SrTiO_3$ (30–33). Thus, they lend themselves to electron doping of the $SrTiO_3$ at the interface. The more substantial challenge would be to dope these wider-band-gap materials (see **Figure 1**) with dopants with sufficiently low ionization energies. Interfaces between $SrTiO_3$ and $SrZrO_3$, doped *n*-type with La or Nb, were recently modeled theoretically and predicted to produce a tightly confined 2DEG (34). Very recent experimental studies, using angle-dependent Shubnikov–de Haas oscillations (which are oscillations of the longitudinal resistance in a quantizing magnetic field) confirmed the existence of a 2DEG in the $SrTiO_3$ at $Sr(Zr,Ti)O_3/SrTiO_3$ interfaces (35). In these structures, the wider-band-gap $Sr(Zr,Ti)O_3$ layer was *n*-type doped with La. These examples demonstrate the feasibility of modulation-doped heterostructures for the perovskite oxides. Further improvements, such as the use of spacer layers, should lead to mobility gains.

An advantage of modulation doping relative to the other approaches discussed below is that the carrier density and confinement of the electron gas can be controlled by varying band offsets and the doping in the modulation doping barrier. 2DEGs at interfaces having any crystallographic orientation are possible. Modulation doping offers a route to very low density 2DEGs. Such low-density 2DEGs are subject to the long-range Coulomb interactions that are responsible for the richness of novel phases and new physics discovered in conventional semiconductor heterostructures. Furthermore, superconductivity appears at low electron concentrations in $SrTiO_3$ (36, 37).

2.2. Polarization and Polar Discontinuities

Two basic mechanisms can give rise to a 2DEG without the need for dopants. The first is based on the bulk properties of materials whose unit cell exhibits a spontaneous electric polarization

(having a point group belonging to one of the 10 polar crystal classes) or an induced polarization via the piezoelectric effect (having a point group belonging to the 20 piezoelectric point groups). A necessary requirement for both is the lack of a center of symmetry. Nitride semiconductors adopt the wurtzite structure with the point group *6mm*, which is piezoelectric and polar. At heterointerfaces, such as those between AlGaN and GaN, a discontinuity in the strain-induced or spontaneous polarization creates internal electrostatic fields and bound interface polarization charges (38, 39). This fixed polarization charge can reach values on the order of 5×10^{13} cm^{-2}, depending on the interface orientation (40), and produces mobile carrier densities of a similar value, without any dopants. It is now understood that the compensating mobile carriers are donated to the 2DEG from donor-like surface states (39). The polarization-induced sheet charge density can furthermore be controlled by the thickness and composition of the AlGaN layer. Polarization doping has several fundamental advantages over modulation doping. Because the electron charge is induced by atomic-scale polarization, devices can be scaled to any dimension, a significant advantage over dopant-based structures, for which dopant solubility and statistics limit scaling. Moreover, polarization charges are highly uniform on every unit cell and do not act as ionized scattering centers for carrier transport (see Reference 3 for a comprehensive discussion of the scattering mechanisms in polarization-induced 2DEGs). The use of polarization discontinuities to generate 2DEGs has been highly successful in oxides as well: The aforementioned high-mobility ZnO/$Mg_xZn_{1-x}O$ wurtzite heterostructures use this mechanism (5, 6). Many of the oxides of interest to this article are centrosymmetric. Notable exceptions are the ferroelectric perovskites, such as $BaTiO_3$ and $PbTiO_3$, which possess a switchable electrical polarization. Very high surface or interface charge densities on the order of 10^{14} cm^{-2} can be induced by using these materials (41–43). A practical challenge is that ferroelectrics exhibit a tendency for polarization loss, due to depolarization and other mechanisms such as charge trapping (44).

2.3. Interfaces Formed Between a Polar Surface and a Nonpolar Surface

Another approach by which to generate a high-mobility 2DEG is to form an interface between two oxides: one with a polar surface and the other with a nonpolar surface. The electrostatics of polar/nonpolar interfaces were first worked out by Harrison and coworkers (45) for Ge/GaAs heteroepitaxy. Later, Hwang and coworkers (46, 47) proposed this approach as a route to 2DEGs at the $LaAlO_3/SrTiO_3$ interface.

The origin of the 2DEG at polar/nonpolar interfaces can be understood by using rather simple considerations (for a formal treatment of the electrostatics of such interfaces, see References 48–50). Take, for example, an interface created by bringing into contact the (001) surfaces of $SrTiO_3$ and a rare earth titanate ($RTiO_3$, where R is a trivalent rare earth ion), as shown in **Figure 2** [we use (pseudo)cubic unit cell notation]. Both materials are insulators in bulk [Ti is in a d^1 configuration in $RTiO_3$, but the materials are Mott insulators with band gaps ranging from 0.1 to 1 eV, depending on the ionic radius of R (51)]. $R^{3+}O^{2-}$ and $Ti^{3+}O_2{}^{4-}$ layers alternate along the surface normal of the $RTiO_3$, carrying formal +1 and −1 charges, respectively. These layers transition abruptly at the interface to a sequence of neutral layers, $Sr^{2+}O^{2-}$ and $Ti^{4+}O_2{}^{4-}$, of nonpolar (001) $SrTiO_3$. A fixed charge arises at the interface. For this system, the interface plane is a TiO_2 plane. The fixed interface charge can be compensated by a 2DEG, bound to the interface by the fixed charge. The charge density in this 2DEG is extremely high, on the order of 3×10^{14} cm^{-2}, as given by $e/2S$, where S is the surface unit cell area and e the elementary charge. This sheet charge density is approximately 10× higher than what is possible even with the polar III–nitride semiconductor heterostructures. Confirming this basic picture, high mobile carrier densities of several 10^{14} cm^{-2} have been observed for a number for $RTiO_3/SrTiO_3$ interfaces (52, 53). Several

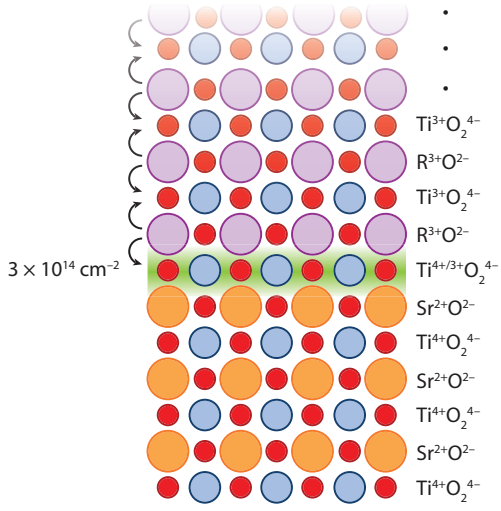

Figure 2

Schematic showing the formation of a two-dimensional electron gas (2DEG) at a prototypical polar/nonpolar oxide interface formed between the (001) surfaces of $SrTiO_3$ and $RTiO_3$. The RO and TiO_2 planes in $RTiO_3$ carry +1 and −1 formal ionic charges, respectively. Each RO layer donates one-half an electron to the upper- and lower-lying TiO_2 planes, including the interfacial TiO_2 plane, where the half-electron forms a mobile 2DEG, as indicated by the arrows. The TiO_2 and SrO layers in the $SrTiO_3$ are charge neutral. The 2DEG, with mobile carrier densities on the order of 3×10^{14} cm^{-2}, compensates for the net fixed positive interface charge carried by the terminating RO plane. The red circles denote O, the orange circles denote Sr, the blue circles denote Ti, and the purple circles denote R.

control experiments can be used to establish that the carriers are indeed due to the interface, rather than from some other source, such as donor-type defects in the bulk or interdiffusion. For example, if some of the trivalent R ions are replaced with a divalent ion such as Sr, then the fixed charge at the interface, and therefore the 2DEG density, should be reduced accordingly. This is indeed observed in experiment (54). Furthermore, $RTiO_3/SrTiO_3$ superlattices exhibit carrier densities that increase by a constant amount of $\sim 3 \times 10^{14}$ cm^{-2} with each additional interface (52, 53), thus confirming that the charge carriers are due to the interface. $SrTiO_3$ layers as thin as ∼1–2 unit cells exhibit the entire $\sim 3 \times 10^{14}$ cm^{-2} sheet carrier density when interfaced with $RTiO_3$ (53, 55, 56).

The origin of the mobile charge at these interfaces has caused some confusion. In contrast to the case for the nitride interfaces described above, the source of charge is the interface itself. Consider, for example, an atomically sharp $RTiO_3/SrTiO_3$ (001) interface, in which the interface plane is TiO_2 (**Figure 2**). In bulk $RTiO_3$, each $R^{3+}O^{2-}$ layer, which carries a +1 formal charge, donates one-half an electron per planar unit cell to the under- and upper-lying TiO_2 planes (see **Figure 2**), which carry formal −1 charges. At the interface, the terminating $R^{3+}O^{2-}$ layer transfers one-half an electron per interface unit cell, or $\sim 3 \times 10^{14}$ cm^{-2}, to the interfacial TiO_2 plane, donating mobile charge to that layer. The origin of the charge is fundamentally and conceptually no different from introducing R^{3+} dopants in $SrTiO_3$, with each R^{3+} donating one electron to the conduction band of $SrTiO_3$ (57), except here we have an entire sheet of such dopants. The band offsets at $RTiO_3/SrTiO_3$ (58) and $LaAlO_3/SrTiO_3$ (31, 32, 59) interfaces are such that the mobile charge resides in the $SrTiO_3$. Although the mobile charge remains attracted to the positive bound charge, forming a confined 2DEG, it spreads over a certain number of layers away from the interface. The degree to which the charge spreads depends on a number of factors and is further discussed below.

Although the 2DEG, at least at interfaces at which the theoretically expected mobile charge density is experimentally observed, perfectly compensates for the bound charge at the interface, some attention must be paid to the free polar surface for structures of type $R\mathrm{TiO_3}/\mathrm{SrTiO_3}$ or $\mathrm{LaAlO_3}/\mathrm{SrTiO_3}$, for which the oxide with the polar surface, i.e., $R\mathrm{TiO_3}$ or $\mathrm{LaAlO_3}$, is the top layer. Specifically, the RO-$\mathrm{TiO_2}$ or LaO-$\mathrm{AlO_2}$ units (bilayers) carry a nonzero dipole moment, which would cause a diverging electrostatic surface energy (60). (This is not an issue for symmetric structures, such as $\mathrm{SrTiO_3}/R\mathrm{TiO_3}/\mathrm{SrTiO_3}$, for which 2DEGs at each interface provide the required compensation.) Polar oxide surfaces are ubiquitous and have been extensively studied both theoretically and experimentally (49, 60, 61). There are many different pathways by which polar surfaces solve their polar problem, including by changing the surface stoichiometry or the valence state of a transition metal ion and/or by adsorbing species such as hydrogen. The degree to which the polar nature of the exposed oxide surface and its passivation influence the 2DEG at an interface that is in close proximity to the 2DEG is a subject of active investigation (31, 62, 63). We do not consider such questions further. That is, we make the reasonable assumptions that the free (top) polar surface, like other polar surfaces, has solved its polar problem by one of the many mechanisms available to such surfaces and that, with the 2DEG compensating for the fixed charge at the interface, there is no diverging electrostatic potential. This picture appears to describe at least $R\mathrm{TiO_3}/\mathrm{SrTiO_3}$ heterostructures extremely well.

2DEGs formed by using nonpolar/polar interfaces share many of the advantages of 2DEGs formed by a polarization discontinuity, which are described in Section 2.2. For an ideal, atomically flat interface, the bound charges are highly uniform on every unit cell and thus do not act as ionized scattering centers for carrier transport. In contrast to the case for modulation doping, the 2DEG sheet carrier density is fixed. The mobile 2DEG charge density may, however, be altered by defects that trap electrons in localized states on either side of the interface, by doping the barrier material [thus reducing the effective positive charge (54)], or by applying an electrical bias to a gate.

$\mathrm{LaAlO_3}/\mathrm{SrTiO_3}$ interfaces are formally equivalent to the $R\mathrm{TiO_3}/\mathrm{SrTiO_3}$ interface discussed above. However, well-oxidized $\mathrm{LaAlO_3}/\mathrm{SrTiO_3}$ interfaces typically show mobile carrier densities that are an order of magnitude lower than the expected density of 3×10^{14} cm^{-2} (16). The reasons for such lower mobile carrier densities are poorly understood and most likely involve some sort of defect-related mechanism. The reduced charge density has caused substantial discussion in the literature about the origin of the conductivity at this interface (31, 33, 59, 64–69).

3. ADVANCES IN MATERIALS SYNTHESIS FOR HIGH-MOBILITY OXIDE INTERFACES

Oxide thin films have been deposited by solution-based methods, sputtering, pulsed laser deposition (PLD), MBE, and metal-organic chemical vapor deposition (MOCVD) (70, 71). Sputtering and PLD are attractive because of their apparent simplicity, cost, high throughput, flexibility in exploring new materials, and ability to use relatively high oxygen pressures. The last factor can be very important for some oxide thin-film systems. They face, however, significant challenges in their ability to produce films with low defect densities, which result from energetic deposition (72) and poor control of thin-film stoichiometry (73). Consider typical levels of stoichiometry, defect, and purity control, on the order of 0.1–1%, which correspond to defect and impurity concentrations of 10^{20} cm^{-3} or higher. This situation sharply contrasts with that for high-quality semiconductor films, for which impurity and point defect concentrations are in the part-per-million range or better, corresponding to concentrations of less than 10^{17} cm^{-3}. The role of high defect concentrations in a wide range of properties of complex oxide thin films is still poorly understood, and some properties are certainly less sensitive to defects than are others. For the

$SrTiO_3$-based oxide interfaces that are the subject of this article, low defect concentrations are of paramount importance because defects can dominate the transport properties.

The low thermal energies of the species in MBE and MOCVD allow for conditions closer to equilibrium, thereby decreasing intrinsic defect concentrations. The poor volatility and thermal stability of some precursors (e.g., Ba and Sr) make the precise delivery of these constituents difficult so that MOCVD growth of many oxides requires significant tool and precursor development (74–77). MBE involves the generation of fluxes (molecular beams) and their reaction on the substrate to form an epitaxial film. The constituents are heated in effusion cells or in electron beam evaporators or are introduced as gases to cause transfer to the heated substrate. To maintain high fluxes and purity, ultrahigh vacuum is needed. MBE of oxide films requires reactive oxygen sources, precise control over beam fluxes and growth temperatures, and oxygen-tolerant metal sources and substrate heaters. Despite many advances, stoichiometry control is still considered a major challenge. The low growth pressures in MBE and practical limitations, such as oxidation of the metal source materials, cause flux instabilities (79, 80) and limit practical oxygen pressures, which in turn can result in oxygen-deficient films. Substantial efforts have been directed toward fully oxidized films; solutions include the use of reactive oxidants such as atomic oxygen, ozone (81), and metal-organic sources that supply metals already bonded to oxygen (82). Cation stoichiometry control has been equally challenging. III–V semiconductors exhibit a wide MBE growth window (sometimes also referred to as adsorption-controlled MBE), in which only the stoichiometric phase grows for a range of fluxes (83). For GaAs, the high volatility of As allows for a growth window that spans many orders of magnitude of As gas pressure (84). Some oxides, in particular those having at least one relatively volatile constituent such as Bi or Pb, also exhibit MBE growth windows (84, 85). Many others, however, do not have a wide MBE growth window if grown by using conventional elemental metal sources, such as Knudsen cells, electron beam evaporators, or sublimation sources. For example, if only stoichiometric $SrTiO_3$ is to condense within a range of metal fluxes, growth conditions must allow excess Sr or SrO to desorb; Ti has a sticking coefficient of nearly one if evaporated from elemental metal sources (84). For these reasons, only a narrow window at very high growth temperatures and impractical low pressures can be obtained (86). Without a practical growth window, MBE of oxides requires precise flux control and stability to obtain a stoichiometric oxide. Despite substantial efforts, flux control is limited on the order of 0.1–1% (87, 88), corresponding to defect concentrations of 10^{20} cm^{-3} or higher. A practical solution is to supply one constituent, such as Ti or Zr, using a volatile metal-organic precursor (35, 82, 89). The volatility of such precursors allows for a growth window in the MBE of a wide range of materials (86, 90), thus resulting in excellent stoichiometry control. For example, carrier densities in La-doped $SrTiO_3$ can be controlled into the low 10^{17} cm^{-3} range (thereby placing an upper limit on electrically active defects) (91, 92), electron mobilities exceed 50,000 cm^2 V^{-1} s^{-1} (see **Figure 3** and Reference 93), and Sr vacancy defects are as low as $\sim 10^{16}$ cm^{-3} (94). The mobilities of these MBE films can be further enhanced to >100,000 cm^2 V^{-1} s^{-1} by using strain engineering (95). These results show that complex oxides can be grown to electronic device quality and with defect concentrations far lower than what would be possible in purely flux-controlled MBE.

4. $SrTiO_3$-BASED TWO-DIMENSIONAL ELECTRON GASES

4.1. Electronic Structure of Bulk $SrTiO_3$

As discussed above, many investigations have focused on 2DEGs in which transport occurs in $SrTiO_3$ at interfaces such as $LaAlO_3/SrTiO_3$ (14–17, 46) and $RTiO_3/SrTiO_3$ (52, 53, 96), among others (69, 97, 98). Therefore, we next discuss briefly the electronic structure of $SrTiO_3$.

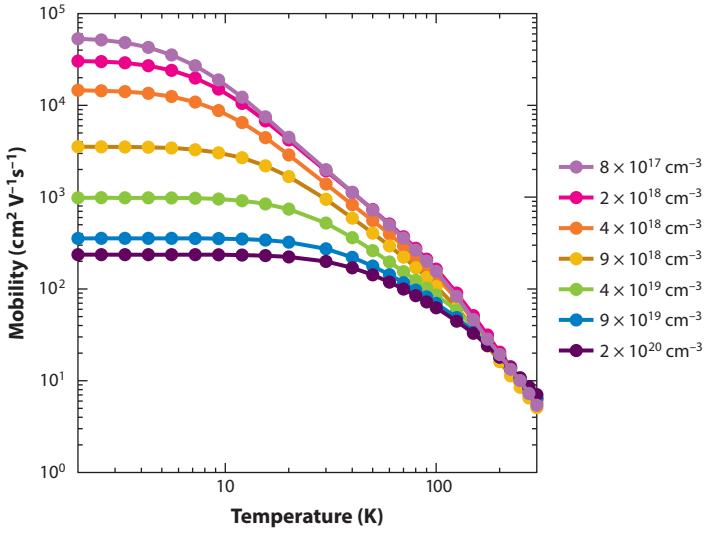

Figure 3

Electron mobilities as a function of carrier density for La-doped $SrTiO_3$ films grown by molecular beam epitaxy. Reprinted with permission from Reference 93. Copyright 2013, American Institute of Physics.

$SrTiO_3$ is a band insulator with a band gap of 3.2 eV (26) separating a conduction band that is derived largely from Ti 3*d* states and a valence band that is derived from O 2*p* states (99). The lowest-lying Ti 3*d* states make up the t_{2g} manifold and are distinguished by their symmetries as t_{xy}, t_{xz}, and t_{yz}. These states are dispersed over ~2 eV and form the basis for the occupied states in $SrTiO_3$-based 2DEGs. Details of the band edge are important. At the Γ point, the threefold degeneracy is lifted by spin-orbit coupling (99) and by the tetragonal, antiferrodistortive distortion (100) of the $SrTiO_3$ unit cell below ~105 K (101). The energy of the spin-orbit split-off band was experimentally measured to be ~17 meV by interband Raman scattering (102). The energy dispersion of the states at the band edge was determined from Shubnikov–de Haas oscillations (92, 103). Comparison of the latter results with band structure calculations (104) implies a transport mass that is enhanced by a factor of two to three relative to the band mass, which is presumably caused by polaronic coupling. This interpretation is consistent with polaron mass enhancement determined by measurements of the extended Drude response (7, 105).

4.2. Theory of Interface Two-Dimensional Electron Gases in $SrTiO_3$

To obtain a 2DEG in $SrTiO_3$ that is electrostatically confined near an interface, two criteria must be satisfied. First, a fixed positive charge must attract the mobile electrons to the interface. Second, the conduction band offset between the two materials must be such that the electrons are kept in the $SrTiO_3$. Such a system is charge neutral; ideally, the total 2DEG electron density in the $SrTiO_3$ neutralizes the fixed positive charge in the interfacing material.

As for conventional semiconductor heterostructures, the electron states of the 2DEG are described quantum mechanically by freely propagating states along the interface and by localized wave functions that describe the spatial extension of the electron gas into the $SrTiO_3$. Microscopic models describe accumulation (106) and assume no band bending or significant electric fields behind the 2DEG. Back gating through thick substrates (109–110) does not compromise this assumption, but inverted structures like those explored for extreme electron density, depletion

mode, and heterostructure field effect transistors (111) are subject to large back-side electric fields that should not be ignored.

The similarities between the 3D valence band structure of III–V semiconductors and the conduction band edge band structure of $SrTiO_3$—specifically, the existence of heavy and light electron (hole) bands and a spin-orbit split-off band—suggest a comparison between the subband structure of quantized hole gases in the III–Vs (112, 113) and $SrTiO_3$ 2DEGs. However, most $SrTiO_3$ 2DEGs currently being investigated have charge densities that are much higher than those typical for conventional semiconductors. As a result, and unlike the case for conventional semiconductors, the energy scale for the subband states in $SrTiO_3$ 2DEGs is much larger than the energy separation from the band edge to the spin-orbit split-off band and is also comparable to or greater than the dispersion of the heavy mass band. In conventional semiconductors, the energy of the twofold-degenerate spin-orbit split-off band is much higher than the subband splittings, and one uses the low-lying fourfold-degenerate manifold to describe the quantization.

Furthermore, $SrTiO_3$ has a high, strongly temperature-dependent, nonlinear, electric field–dependent dielectric constant due to a soft optical phonon mode (114), which needs to be taken into account in the models (46, 115, 116). The dielectric screening in the $SrTiO_3$ is also probably sensitive to the spatial length scales over which the fields vary. At the interface, the effective field will be large and vary rapidly over just several unit cells.

Several theoretical descriptions now exist for the subband structure and electron distribution for 2DEGs in $SrTiO_3$ and have been obtained by using techniques such as density functional theory and tight-binding calculations (31, 34, 48, 115–127). The 2DEG density controls the subband quantization and Fermi surfaces. Many of the theoretical calculations consider interfaces having a carrier density on the order of $\sim 3 \times 10^{14}$ cm^{-2}, which is the theoretically expected density for a polar/nonpolar interface. The results are similar but differ in detail. **Figure 4**, calculated as described in Reference 115, shows the subband states for a 2DEG with a high electron density of $\sim 3 \times 10^{14}$ cm^{-2} and dispersing in the plane of the interface (**Figure 4*b***) and the complex Fermi surface produced by the occupied subbands (**Figure 4*a***). All theoretical models find that the lowest electric subband state is derived from the t_{xy} states. This result can be understood by the fact that in the bulk this state has low dispersion in the k_z direction (which is the surface-normal direction here), leading to a very large effective mass. Quantum confinement adds the least kinetic energy while minimizing the electrostatic potential energy. For high-density 2DEGs, this state is separated from the next excited state by ~160 to 270 meV. At slightly higher energies is a dense manifold of subband states. The range of calculated energies to the next excited state given here reflects the variation in results from different calculations in the literature (48, 116, 120, 122, 127). We note the very close energy spacings of the manifold of higher-lying subbands (see **Figure 4**). The Fermi surface is described by a series of circles originating from the t_{xy} subbands and ellipses derived from the t_{xz} and t_{yz} subbands. The spin-orbit interaction is manifested in the weak orbit repulsion as the circles and ellipses cross each other. At high 2DEG densities, ~0.5 electrons per interface unit cell, roughly half of the electrons are in t_{xy} states, whereas the remainder are distributed between the t_{xz} and t_{yz} states. The wave function for the lowest-lying t_{xy} state extends approximately one unit cell into the $SrTiO_3$; these electrons are confined to one TiO_2 plane. Higher-energy t_{xz} and t_{yz} states describe a tail of charge that spreads deep into the substrate (115, 116). Even at much lower electron densities, i.e., $\sim 10^{12}$ cm^{-2}, multiple subbands are expected to be occupied (115).

4.3. Two-Dimensional Electron Gases in $SrTiO_3$: Experimental Results

Experimental work on $SrTiO_3$ 2DEGs has focused on measurements of subband energies, shapes of the Fermi surfaces, effective masses, and potential magnetism and superconducting properties

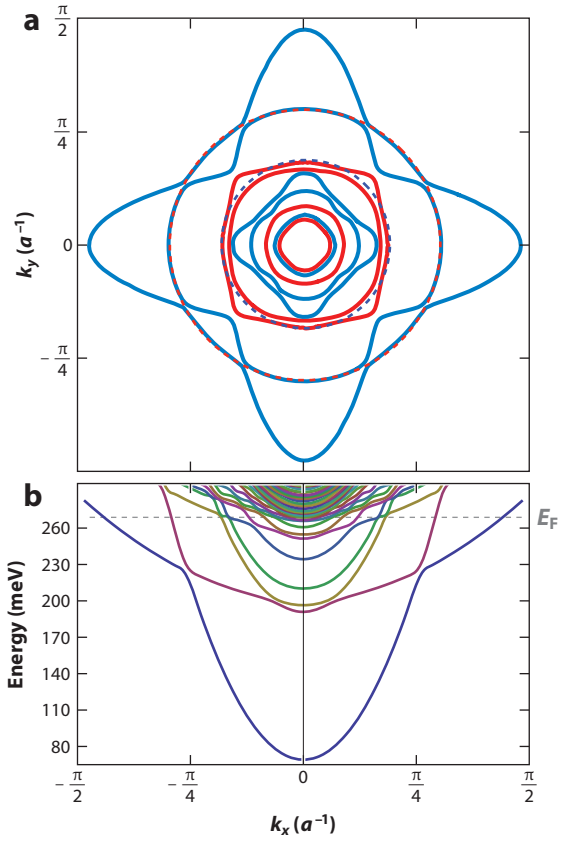

Figure 4

(*a*) Theoretical calculations of the Fermi surfaces and (*b*) 2D band structure of a 2DEG in $SrTiO_3$ for a sheet carrier density of 3.2×10^{14} cm^{-2}. In panel *a*, the dominant orbital character at the Γ point is represented by blue for t_{xy} and by red for t_{yz} and t_{xz}. Possible magnetic breakdown orbits are shown in dashed lines of opposite color. In panel *b*, the Fermi energy is indicated by the gray, dashed, horizontal line. Figure calculated as described in Reference 115 and courtesy of Guru Khalsa.

of this high-electron-density 2D system. As is described below, measurements of the subband states are challenging, and the experimental understanding is still evolving. A second important focus is the control of 2DEGs by applied electric fields.

4.3.1. Subband states. Angle-resolved photoemission spectroscopy (ARPES) has been used to resolve electric subbands, the in-plane dispersion, and Fermi wave vectors for electronic states at $SrTiO_3$ surfaces (128). Results reported in Reference 128 show two parabolas separated by ~0.15 eV that may be assigned to the two lowest-lying t_{xy} subbands. The dispersion corresponds to an effective mass on the order of ~0.6 m_e, which is in reasonable accord with the results for band structure calculations of $SrTiO_3$ (104). Without an independent measure of the surface electron density, these measurements cannot test the model calculations described in Section 4.2. ARPES has also been used to measure the electron surface states of pulsed laser–deposited $SrTiO_3$ (129). The $SrTiO_3$ film is deposited onto $LaTiO_3$, which is a Mott insulator and induces a high-density 2DEG in $SrTiO_3$ at the common interface (52). The electron states at the exposed surface evolve and develop a Fermi surface intimately related to $SrTiO_3$ band structure (129). The results

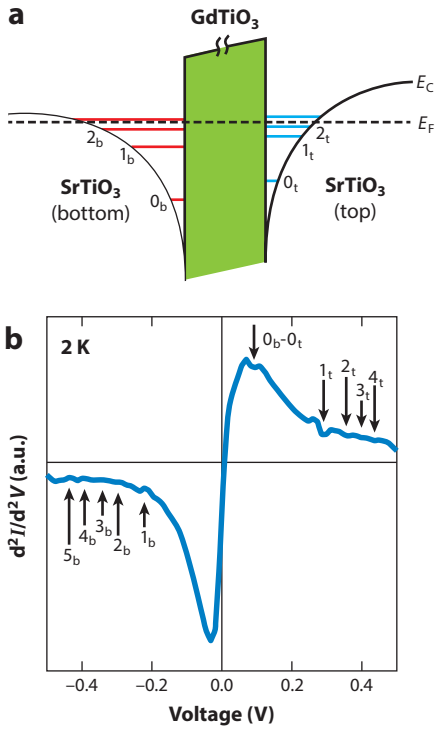

Figure 5

(*a*) Schematic energy diagram of the subband configuration of a $SrTiO_3/GdTiO_3/SrTiO_3$ heterostructure at zero applied bias and low temperature. The $GdTiO_3$ is the tunnel barrier. A slight asymmetry in the carrier concentration and resulting subband spacing between the two 2DEGs is assumed. The subbands and band bending shown are for illustrative purposes only, and the schematic is not meant to be quantitative. E_C indicates the conduction band edge, and E_F (*dashed line*) denotes the Fermi level. In both panels *a* and *b*, the numbers (e.g., 0, 1, 2) refer to the subband indices, and the subscripts t and b refer to top and bottom 2DEGs, respectively. (*b*) Experimentally measured d^2I/d^2V characteristics of a $SrTiO_3/GdTiO_3/SrTiO_3$ resonant tunneling heterostructure at 2 K. Features due to resonant tunneling between the subbands are indicated by arrows. Reprinted with permission from Reference 132. Copyright 2013, American Institute of Physics.

emphasize the tight binding of the states, a few unit cells of $SrTiO_3$, to the $LaTiO_3$ but do not provide a quantitative test of the aforementioned theoretical models.

A direct method of probing 2DEG subband structures involves resonant tunneling between two parallel 2DEGs separated by a tunnel barrier (130, 131). A recent study of tunneling between two 2DEGs in $SrTiO_3$ on either side of a relatively thin barrier of $GdTiO_3$ revealed resonances that appear at the specific applied biases that cause the subbands in the two 2DEGs to line up (**Figure 5**) (132). Near 0 V, a resonant feature indicates alignment of the ground states of the emitter and collector. At higher voltages, new features indicate alignment of the ground state in one 2DEG with the excited states of the second. Conservation of in-plane momentum requires that the collector states have the same symmetry as the ground state in the emitter; that is, tunneling occurs between subbands of t_{xy} character. The results can be interpreted in terms of the separation between the lowest-lying subband and the second-lowest subband, of 210 and 310 meV, respectively, for the two 2DEGs. The difference in the separations between the two lowest-lying subbands in the two 2DEGs is due to a difference in their carrier densities, which were measured

independently by using Hall measurements (132). The results thus confirm that subband spacings and carrier confinement very sensitively depend on the carrier density, as expected. At slightly higher voltage, dense features may be identified with the spectrum of closely spaced high-lying subband states. The results thus agree substantially with the theoretical predictions, as described in Section 4.2.

Application of voltage systematically changes the effective electron density in the interface layer (110). The changes in the subband states induced by a back gate through a thick substrate, which is frequently employed (107–110), should be different from changes produced by a front-side gate or produced by altering the net interfacial positive charge (106, 133, 134). In the latter situation, the space charge that determines the electric quantization may be described by accumulation with no back-side electric field. For negative back-side voltage, the 2DEG density is reduced, and the tails of the subband wave functions experience a stronger confining potential. For a positive back-side voltage, the kinetic effects of quantum confinement are reduced, tails are extended, and the occupation of t_{xz} and t_{yz} is enhanced. As a result, dramatic changes in transport occur with increasing back-gate bias. Superconductivity, an enhanced Rashba coefficient, a Hall resistance that is nonlinear in magnetic field, and anomalous metallic behavior appear at high positive back-gate voltage (135–138). The critical density associated with the occupation of the t_{xz} and t_{yz} subbands was documented to be $\sim$1.5–2.0 $\times$ 10^{13} cm^{-2} for $LaAlO_3/SrTiO_3$ interfaces grown by PLD (135, 139).

4.3.2. Fermi surfaces. Shubnikov–de Haas oscillations provide a measure of the Fermi surface dimensions and establish the 2D character of an electron gas. The Shubnikov–de Haas oscillation period for a 2D system depends only on the component of the magnetic field that is perpendicular to the plane.

Figure 6 shows oscillations observed from a high-density 2DEG at a $GdTiO_3/SrTiO_3$ interface (140). The periodicity of the oscillations is clear, and the angle dependence (140) establishes the 2D character. The data may be interpreted as arising either from a single subband displaying spin splitting or from two subbands. In either case, the Shubnikov–de Haas densities correspond

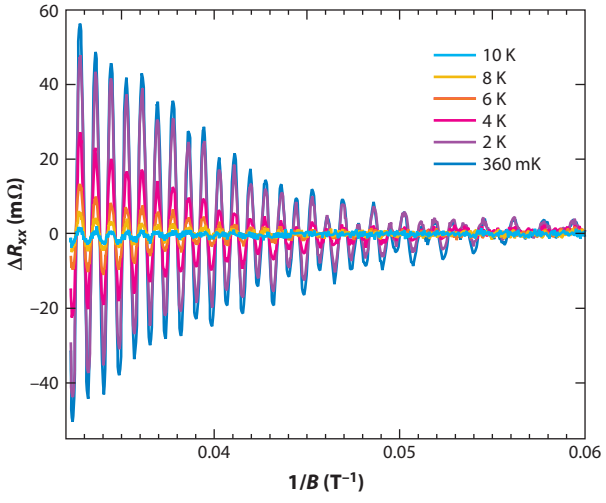

Figure 6

Temperature-dependent Shubnikov–de Haas oscillations from a two-dimensional electron gas at a $SrTiO_3/GdTiO_3$ interface. Reprinted with permission from Reference 140. Copyright 2012, American Institute of Physics.

to only a fraction, 10% or 30%, respectively, of the carrier density measured by the Hall effect ($\sim 3 \times 10^{14}$ cm^{-2}). Given the subband structure of these 2DEGs (see **Figures 3** and **4**), which consists of a low-lying t_{xy} subband well separated in energy, and the very close spacings of the higher-lying subbands, observing Shubnikov–de Haas oscillations from any subband except the lowest-lying subband is likely difficult. However, the electrons in this lowest t_{xy} subband are confined to within one layer at the interface and should experience very strong interface roughness scattering. The oscillation period can be related to a Fermi surface area, and the area(s) derived from **Figure 6** is substantially smaller than the largest and most prominent orbits shown in **Figure 3**. However, if one pursues a model of a single electric subband, spin split in the quantizing magnetic field, and compares this model with the existing models of the subband states, one may conclude that the Fermi surface corresponds to the first excited t_{xy} subband, that the electron mass that describes the conductivity in this plane is $\sim 0.55\ m_e$, and that the g-factor is ~ 2. This subband is one layer removed from the interface and should experience less interface scattering than does the ground state. At present, however, a complete interpretation of the oscillations is still lacking.

Measurements of the Shubnikov–de Haas effect for the $LaAlO_3/SrTiO_3$ and $SrTiO_3/La{:}SrTi_{1-x}Zr_xO_3$ systems exposed the same systematic discrepancy between the electron densities determined by the quantum oscillations and the Hall effect: Only a small fraction of the Hall density gives rise to the oscillations (35, 141–143). Two explanations can be offered. First, other Fermi surface orbits suffer elastic scattering and/or magnetic breakdown between intersecting paths and cannot complete the phase-coherent circulation needed for quantum oscillations. Second, the many subbands and the plethora of related orbits with varying areas are unresolved, leaving only quantum oscillations from the largest extremal orbit. A quantitative interpretation of the results from quantum oscillation measurements in terms of existing theoretical models of the subband structure and Fermi surfaces currently remains elusive.

4.3.3. Rashba spin-orbit coupling. As discussed above, at high 2DEG densities the t_{xz} and t_{yz} subbands appear to play a key role in magnetotransport. In concert with Rashba spin-orbit coupling, the quasi-1D-like transport in each of the t_{xz} and t_{yz} subbands gives rise to a conductance that oscillates with orientation of the in-plane magnetic field (136, 137, 144). By implication, transport at the Fermi energy involves a complex of t_{2g} states interacting with each other via spin-orbit coupling (145). Rashba spin-orbit coupling is measured independently by the contributions to weak localization and antilocalization and grows with increasing electron density by more than an order of magnitude, as the 2DEG involves multi-t_{2g} transport and supports superconductivity (136). Recent theories (121, 122) support the notion that multiorbital effects, at play for high interface electron densities, account for the Rashba splittings on the order of tens of millielectron volts that are deduced from experiments (136, 137, 144). Experiment (146) and theory (122) support the notion of a Rashba effect cubic in the in-plane momentum.

4.3.4. Confined quantum wells. Narrow $SrTiO_3$ quantum wells bound by $GdTiO_3$ barriers on either side contain a very high 2DEG density of $\sim 7 \times 10^{14}$ cm^{-2} carriers. As the quantum well thickness is reduced, the effective 3D electron density increases. Such structures were recently used (experimentally and theoretically) as model systems to study the effects arising from electron correlations in $SrTiO_3$-based 2DEGs (55, 147). Specifically, short-range Coulomb interactions are expected to become important at high densities, as the probability that two electrons occupy the same site grows. Such Coulomb interactions are manifested in an upturn in the T^2 dependence of the resistivity as the quantum well thickness shrinks, signaling mass enhancement and the approach to a 2D Mott insulator (55). At approximately the same thickness, proximity-induced ferromagnetism appears in the quantum well 2DEG (148). At the smallest dimension (quantum

wells that contain just two layers of SrO), the 2D system localizes, despite the high local doping density, and forms a high-density gas of self-trapped small polarons (149). As is the case for bulk Mott-insulating rare earth titanates, the localization is coupled with distortions of Ti-O octahedra (150). These results open up the exciting possibility of controllably engineering unusual states of matter in 2D systems by using proximity effects and electrostatic doping.

5. SUMMARY AND OUTLOOK

Substantial advances have recently been made in the understanding of 2DEGs in $SrTiO_3$. In particular, experiment and theory qualitatively agree with respect to the subband structure in high-density 2DEGs, which should enable rapid advances in the design of quantum-confined structures with $SrTiO_3$ that exhibit novel phenomena. Experimentally, however, further improvements in the mobility of 2DEGs in $SrTiO_3$ are needed. Although thin films with mobilities exceeding those of single crystals can now routinely be grown by MBE, the corresponding 2DEG mobilities are significantly lacking, likely because of a multitude of reasons. Approaches such as modulation doping need to be pursued. One of the most exciting aspects of 2DEGs in $SrTiO_3$ is the exploration of interactions caused by strong electron correlations due to short-range Coulomb repulsions of the conducting electrons within electrostatically doped structures. Just as heterostructure band structure engineering is a crowning achievement of conventional semiconductor physics and devices, oxide heterostructures that allow for engineering and controlling correlation physics may lead to new scientific and technological arenas.

DISCLOSURE STATEMENT

The authors are not aware of any affiliations, memberships, funding, or financial holdings that might be perceived as affecting the objectivity of this review.

ACKNOWLEDGMENTS

We acknowledge discussions and collaborations with Leon Balents, Tyler Cain, David Goldhaber-Gordon, Jinwoo Hwang, Clayton Jackson, Anderson Janotti, Adam Kajdos, Guru Khalsa, Allan MacDonald, Pouya Moetakef, Dan Ouellette, Santosh Raghavan, Siddharth Rajan, Chris Van de Walle, Jimmy Williams, and Jack Zhang. The authors acknowledge funding from a Multidisciplinary University Research Initiative (MURI) program of the Army Research Office (grant number W911-NF-09-1-0398), from the US National Science Foundation (grant numbers DMR-1006640 and DMR-1121053), from the US Department of Energy (award number DE-FG02-02ER45994), and from DARPA (award number W911NF-12-1-0574).

LITERATURE CITED

1. Tsui DC, Stormer HL, Gossard AC. 1982. Two-dimensional magnetotransport in the extreme quantum limit. *Phys. Rev. Lett.* 48:1559–62
2. Pfeiffer L, West KW. 2003. The role of MBE in recent quantum Hall effect physics discoveries. *Physics E* 20:57–64
3. Jena D. 2008. Polarization effects on low-field transport & mobility in III–V nitride HEMTs. In *Polarization Effects in Semiconductors*, ed. C Wood, D Jena, pp. 161–216. New York: Springer
4. Singh J. 2003. *Electronic and Optoelectronic Properties of Semiconductor Structures*. Cambridge, UK: Cambridge Univ. Press

5. Tsukazaki A, Ohtomo A, Kita T, Ohno Y, Ohno H, Kawasaki M. 2007. Quantum Hall effect in polar oxide heterostructures. *Science* 315:1388–91
6. Tsukazaki A, Akasaka S, Nakahara K, Ohno Y, Ohno H, et al. 2010. Observation of the fractional quantum Hall effect in an oxide. *Nat. Mater.* 9:889–93
7. van der Marel D, van Mechelen JLM, Mazin II. 2011. Common Fermi-liquid origin of T^2 resistivity and superconductivity in *n*-type $SrTiO_3$. *Phys. Rev. B* 84:205111
8. Frederikse HPR, Hosler WR. 1967. Hall mobility in $SrTiO_3$. *Phys. Rev.* 161:822–27
9. Cox PA. 1992. *Transition Metal Oxides*. Oxford, UK: Clarendon
10. Mott NF. 1949. The basis of the electron theory of metals, with special reference to the transition metals. *Proc. Phys. Soc. A* 62:416–22
11. Imada M, Fujimori A, Tokura Y. 1998. Metal-insulator transitions. *Rev. Mod. Phys.* 70:1039–263
12. Bhattacharya A, May S. 2014. Magnetic oxide heterostructures. *Annu. Rev. Mater. Res.* 44:65–90
13. Ngai JH, Walker FJ, Ahn CH. 2014. Correlated oxide physics and electronics. *Annu. Rev. Mater. Res.* 44:1–17
14. Mannhart J, Blank DHA, Hwang HY, Millis AJ, Triscone J-M. 2008. Two-dimensional electron gases at oxide interfaces. *MRS Bull.* 33:1027–34
15. Mannhart J, Schlom DG. 2010. Oxide interfaces: an opportunity for electronics. *Science* 327:1607–11
16. Huijben M, Brinkman A, Koster G, Rijnders G, Hilgenkamp H, Blank DHA. 2009. Structure-property relation of $SrTiO_3/LaAlO_3$ interfaces. *Adv. Mater.* 21:1665–77
17. Zubko P, Gariglio S, Gabay M, Ghosez P, Triscone J-M. 2011. Interface physics in complex oxide heterostructures. *Annu. Rev. Condens. Matter Phys.* 2:141–65
18. Schlom DG, Haeni JH, Lettieri J, Theis CD, Tian W, et al. 2001. Oxide nano-engineering using MBE. *Mater. Sci. Eng. B* 87:282–91
19. Schlom DG, Chen LQ, Pan XQ, Schmehl A, Zurbuchen MA. 2008. A thin film approach to engineering functionality into oxides. *J. Am. Ceram. Soc.* 91:2429–54
20. Dingle R, Stormer HL, Gossard AC, Wiegmann W. 1978. Electron mobilities in modulation-doped semiconductor heterojunction superlattices. *Appl. Phys. Lett.* 33:665–67
21. Eisenstein JP, Cooper KB, Pfeiffer LN, West KW. 2002. Insulating and fractional quantum Hall states in the first excited Landau level. *Phys. Rev. Lett.* 88:076801
22. Umansky V, Heiblum M, Levinson Y, Smet J, Nubler J, Dolev M. 2009. MBE growth of ultra-low disorder 2DEG with mobility exceeding 35×10^6 cm^2/V s. *J. Cryst. Growth* 311:1658–61
23. Mimura T, Hiyamizu S, Fujii T, Nanbu K. 1980. A new field-effect transistor with selectively doped GaAs/*n*-$Al_xGa_{1-x}As$ heterojunctions. *Jpn. J. Appl. Phys.* 19:L225–27
24. Delagebeaudeuf D, Linh NT. 1982. Metal-(*n*) AlGaAs-GaAs two-dimensional electron gas FET. *IEEE Trans. Electron. Devices* 29:955–60
25. Zunger A, Kilic C, Wang L. 2002. Defects in photovoltaic materials and the origin of failure to dope them. *Proc. IEEE Photovoltaic Spec. Conf., 29th, New Orleans*, 2002:500–3
26. van Benthem K, Elsässer C, French RH. 2001. Bulk electronic structure of $SrTiO_3$: experiment and theory. *J. Appl. Phys.* 90:6156–64
27. Lim SG, Kriventsov S, Jackson TN, Haeni JH, Schlom DG, et al. 2002. Dielectric functions and optical bandgaps of high-K dielectrics for metal-oxide-semiconductor field-effect transistors by far ultraviolet spectroscopic ellipsometry. *J. Appl. Phys.* 91:4500–5
28. Derks C, Kuepper K, Raekers M, Postnikov AV, Uecker R, et al. 2012. Band-gap variation in $RScO_3$ (R = Pr, Nd, Sm, Eu, Gd, Tb, and Dy): X-ray absorption and O *K*-edge X-ray emission spectroscopies. *Phys. Rev. B* 86:155124
29. Lee YS, Lee JS, Noh TW, Byun DY, Yoo KS, et al. 2003. Systematic trends in the electronic structure parameters of the 4*d* transition-metal oxides $SrMO_3$ (M = Zr, Mo, Ru, and Rh). *Phys. Rev. B* 67:113101
30. Schafranek R, Baniecki JD, Ishii M, Kotaka Y, Yamanka K, Kurihara K. 2012. Band offsets at the epitaxial $SrTiO_3/SrZrO_3$ (0 0 1) heterojunction. *J. Phys. D* 45:055303
31. Janotti A, Bjaalie L, Gordon L, Van de Walle CG. 2012. Controlling the density of the two-dimensional electron gas at the $SrTiO_3/LaAlO_3$ interface. *Phys. Rev. B* 86:241108
32. Berner G, Müller A, Pfaff F, Walde J, Richter C, et al. 2013. Band alignment in $LaAlO_3/SrTiO_3$ oxide heterostructures inferred from hard X-ray photoelectron spectroscopy. *Phys. Rev. B* 88:115111

33. Chambers SA, Engelhard MH, Shutthanandan V, Zhu Z, Droubay TC, et al. 2010. Instability, intermixing and electronic structure at the epitaxial $LaAlO_3/SrTiO_3$ heterojunction. *Surf. Sci. Rep.* 65:317–52
34. Delugas P, Filippetti A, Gadaleta A, Pallecchi I, Marré D, Fiorentini V. 2013. Large band offset as driving force of two-dimensional electron confinement: the case of $SrTiO_3/SrZrO_3$ interface. *Phys. Rev. B* 88:115304
35. Kajdos AP, Ouellette DG, Cain TA, Stemmer S. 2013. Two-dimensional electron gas in a modulation-doped $SrTiO_3/Sr(Ti, Zr)O_3$ heterostructure. *Appl. Phys. Lett.* 103:082120
36. Schooley JF, Hosler WR, Cohen ML. 1964. Superconductivity in semiconducting $SrTiO_3$. *Phys. Rev. Lett.* 12:474–75
37. Lin X, Zhu ZW, Fauque B, Behnia K. 2013. Fermi surface of the most dilute superconductor. *Phys. Rev. X* 3:021002
38. Ambacher O, Smart J, Shealy JR, Weimann NG, Chu K, et al. 1999. Two-dimensional electron gases induced by spontaneous and piezoelectric polarization charges in N- and Ga-face AlGaN/GaN heterostructures. *J. Appl. Phys.* 85:3222–33
39. Ibbetson JP, Fini PT, Ness KD, DenBaars SP, Speck JS, Mishra UK. 2000. Polarization effects, surface states, and the source of electrons in AlGaN/GaN heterostructure field effect transistors. *Appl. Phys. Lett.* 77:250–52
40. Speck JS, Chichibu SF. 2009. Nonpolar and semipolar group III nitride-based materials. *MRS Bull.* 34:304–9
41. Ahn CH, Bhattacharya A, Di Ventra M, Eckstein JN, Frisbie CD, et al. 2006. Electrostatic modification of novel materials. *Rev. Mod. Phys.* 78:1185–212
42. Ahn CH, Gariglio S, Paruch P, Tybell T, Antognazza L, Triscone J-M. 1999. Electrostatic modulation of superconductivity in ultrathin $GdBa_2Cu_3O_{7-x}$ films. *Science* 284:1152–55
43. Wu YR, Singh J. 2005. Polar heterostructure for multifunction devices: theoretical studies. *IEEE Trans. Electron. Devices* 52:284–93
44. Hoffman J, Pan XA, Reiner JW, Walker FJ, Han JP, et al. 2010. Ferroelectric field effect transistors for memory applications. *Adv. Mater.* 22:2957–61
45. Harrison WA, Kraut EA, Waldrop JR, Grant RW. 1978. Polar heterojunction interfaces. *Phys. Rev. B* 18:4402–10
46. Ohtomo A, Hwang HY. 2004. A high-mobility electron gas at the $LaAlO_3/SrTiO_3$ heterointerface. *Nature* 427:423–26
47. Nakagawa N, Hwang HY, Muller DA. 2006. Why some interfaces cannot be sharp. *Nat. Mater.* 5:204–9
48. Stengel M. 2011. First-principles modeling of electrostatically doped perovskite systems. *Phys. Rev. Lett.* 106:136803
49. Stengel M. 2011. Electrostatic stability of insulating surfaces: theory and applications. *Phys. Rev. B* 84:205432
50. Bristowe NC, Ghosez P, Littlewood PB, Artacho E. 2013. Origin of two-dimensional electron gases at oxide interfaces: insights from theory. arXiv:1310.8427 [cond-mat.mes-hall]
51. Crandles DA, Timusk T, Garrett JD, Greedan JE. 1992. The mid infrared absorption in $RTiO_3$ perovskites (R = La, Ce, Pr, Nd, Sm, Gd): the Hubbard gap? *Physica C* 201:407–12
52. Kim JS, Seo SSA, Chisholm MF, Kremer RK, Habermeier HU, et al. 2010. Nonlinear Hall effect and multichannel conduction in $LaTiO_3/SrTiO_3$ superlattices. *Phys. Rev. B* 82:201407
53. Moetakef P, Cain TA, Ouellette DG, Zhang JY, Klenov DO, et al. 2011. Electrostatic carrier doping of $GdTiO_3/SrTiO_3$ interfaces. *Appl. Phys. Lett.* 99:232116
54. Cain TA, Moetakef P, Jackson CA, Stemmer S. 2012. Modulation doping to control the high-density electron gas at a polar/non-polar oxide interface. *Appl. Phys. Lett.* 101:111604
55. Moetakef P, Jackson CA, Hwang J, Balents L, Allen SJ, Stemmer S. 2012. Toward an artificial Mott insulator: correlations in confined high-density electron liquids in $SrTiO_3$. *Phys. Rev. B* 86:201102(R)
56. Cain TA, Lee S, Moetakef P, Balents L, Stemmer S, Allen SJ. 2012. Seebeck coefficient of a quantum confined, high-electron-density electron gas in $SrTiO_3$. *Appl. Phys. Lett.* 100:161601
57. Tokura Y, Taguchi Y, Okada Y, Fujishima Y, Arima T, et al. 1993. Filling dependence of electronic properties on the verge of metal-Mott-insulator transition in $Sr_{1-x}La_xTiO_3$. *Phys. Rev. Lett.* 70:2126–29

58. Conti G, Kaiser AM, Gray AX, Nemsak S, Palsson GK, et al. 2013. Band offsets in complex-oxide thin films and heterostructures of $SrTiO_3/LaNiO_3$ and $SrTiO_3/GdTiO_3$ by soft and hard X-ray photoelectron spectroscopy. *J. Appl. Phys.* 113:143704
59. Qiao L, Droubay TC, Kaspar TC, Sushko PV, Chambers SA. 2011. Cation mixing, band offsets and electric fields at $LaAlO_3/SrTiO_3$(001) heterojunctions with variable La:Al atom ratio. *Surf. Sci.* 605:1381–87
60. Noguera C. 2000. Polar oxide surfaces. *J. Phys. Condens. Matter* 12:R367–410
61. Tasker PW. 1979. Stability of ionic crystal surfaces. *J. Phys. C* 12:4977–84
62. Bristowe NC, Littlewood PB, Artacho E. 2011. Surface defects and conduction in polar oxide heterostructures. *Phys. Rev. B* 83:205405
63. Bi F, Bogorin DF, Cen C, Bark CW, Park JW, et al. 2010. "Water-cycle" mechanism for writing and erasing nanostructures at the $LaAlO_3/SrTiO_3$ interface. *Appl. Phys. Lett.* 97:173110
64. Siemons W, Koster G, Yamamoto H, Harrison WA, Lucovsky G, et al. 2007. Origin of charge density at $LaAlO_3$ on $SrTiO_3$ heterointerfaces: possibility of intrinsic doping. *Phys. Rev. Lett.* 98:196802
65. Chambers SA. 2011. Understanding the mechanism of conductivity at the $LaAlO_3/SrTiO_3$(001) interface. *Surf. Sci.* 605:1133–40
66. Schlom DG, Mannhart J. 2011. Oxide electronics: Interface takes charge over Si. *Nat. Mater.* 10:168–69
67. Chen YZ, Christensen DV, Trier F, Pryds N, Smith A, Linderoth S. 2012. On the origin of metallic conductivity at the interface of $LaAlO_3/SrTiO_3$. *Appl. Surf. Sci.* 258:9242–45
68. Kalabukhov A, Gunnarsson R, Borjesson J, Olsson E, Claeson T, Winkler D. 2007. Effect of oxygen vacancies in the $SrTiO_3$ substrate on the electrical properties of the $LaAlO_3/SrTiO_3$ interface. *Phys. Rev. B* 75:121404
69. Chen YZ, Pryds N, Kleibeuker JE, Koster G, Sun JR, et al. 2011. Metallic and insulating interfaces of amorphous $SrTiO_3$-based oxide heterostructures. *Nano Lett.* 11:3774–78
70. Posadas AB, Lippmaa M, Walker FJ, Dawber M, Ahn CH, Triscone J-M. 2007. Growth and novel applications of epitaxial oxide thin films. In *Physics of Ferroelectrics: A Modern Perspective*, ed. KM Rabe, CH Ahn, J-M Triscone, 105:219–304. Berlin: Springer-Verlag
71. Chambers SA. 2010. Epitaxial growth and properties of doped transition metal and complex oxide films. *Adv. Mater.* 22:219–48
72. Cuomo JJ, Pappas DL, Bruley J, Doyle JP, Saenger KL. 1991. Vapor deposition processes for amorphous carbon films with sp^3 fractions approaching diamond. *J. Appl. Phys.* 70:1706–11
73. Ohnishi T, Shibuya K, Yamamoto T, Lippmaa M. 2008. Defects and transport in complex oxide thin films. *J. Appl. Phys.* 103:103703
74. Dhote AM, Meier AL, Towner DJ, Wessels BW, Ni J, Marks TJ. 2005. Low temperature deposition of epitaxial $BaTiO_3$ films in a rotating disk vertical MOCVD reactor. *J. Vac. Sci. Technol. B* 23:1674–78
75. Teren AR, Belot JA, Edleman NL, Marks TJ, Wessels BW. 2000. MOCVD of epitaxial $BaTiO_3$ films using a liquid barium precursor. *Chem. Vapor Depos.* 6:175–77
76. Boyd DA, Hirsch SG, Hubbard C, Cole MW. 2009. BST films grown by metal organic chemical vapor deposition incorporating real-time control of stoichiometry. *Integr. Ferroelectr.* 111:17–26
77. VanBuskirk PC, Bilodeau SM, Roeder JF, Kirlin PS. 1996. Metalorganic chemical vapor deposition of complex metal oxide thin films by liquid source chemical vapor deposition. *Jpn. J. Appl. Phys.* 35:2520–25
78. Wessels BW. 1995. Metal-organic chemical vapor deposition of ferroelectric oxide thin films for electronic and optical applications. *Annu. Rev. Mater. Sci.* 25:525–46
79. Hellman ES, Hartford EH. 1994. Effects of oxygen on the sublimation of alkaline earths from effusion cells. *J. Vac. Sci. Technol. B* 12:1178–80
80. Theis CD, Schlom DG. 1996. Cheap and stable titanium source for use in oxide molecular beam epitaxy systems. *J. Vac. Sci. Technol. A* 14:2677–79
81. Berkley DD, Johnson BR, Anand N, Beauchamp KM, Conroy LE, et al. 1988. In situ formation of superconducting $YBa_2Cu_3O_{7-x}$ thin films using pure ozone vapor oxidation. *Appl. Phys. Lett.* 53:1973–75
82. Jalan B, Engel-Herbert R, Wright NJ, Stemmer S. 2009. Growth of high-quality $SrTiO_3$ films using a hybrid molecular beam epitaxy approach. *J. Vac. Sci. Technol. A* 27:461–64

83. Tsao JY. 1993. *Materials Fundamentals of Molecular Beam Epitaxy*. Boston: Academic
84. Theis CD, Yeh J, Schlom DG, Hawley ME, Brown GW. 1998. Adsorption-controlled growth of $PbTiO_3$ by reactive molecular beam epitaxy. *Thin Solid Films* 325:107–14
85. Lee JH, Ke X, Misra R, Ihlefeld JF, Xu XS, et al. 2010. Adsorption-controlled growth of $BiMnO_3$ films by molecular-beam epitaxy. *Appl. Phys. Lett.* 96:262905
86. Jalan B, Moetakef P, Stemmer S. 2009. Molecular beam epitaxy of $SrTiO_3$ with a growth window. *Appl. Phys. Lett.* 95:032906
87. Haeni JH, Theis CD, Schlom DG. 2000. RHEED intensity oscillations for the stoichiometric growth of $SrTiO_3$ thin films by reactive molecular beam epitaxy. *J. Electroceram.* 4:385–91
88. Klausmeier-Brown ME, Eckstein JN, Bozovic I, Virshup GF. 1992. Accurate measurement of atomic beam flux by pseudo double beam atomic absorption spectroscopy for growth of thin film oxide superconductors. *Appl. Phys. Lett.* 60:657–59
89. Jalan B, Engel-Herbert R, Cagnon J, Stemmer S. 2009. Growth modes in metal-organic molecular beam epitaxy of TiO_2 on *r*-plane sapphire. *J. Vac. Sci. Technol. A* 27:230–33
90. Moetakef P, Zhang JY, Raghavan S, Kajdos AP, Stemmer S. 2013. Growth window and effect of substrate symmetry in hybrid molecular beam epitaxy of a Mott insulating rare earth titanate. *J. Vac. Sci. Technol. A* 31:041503
91. Son J, Moetakef P, Jalan B, Bierwagen O, Wright NJ, et al. 2010. Epitaxial $SrTiO_3$ films with electron mobilities exceeding 30,000 $cm^2\ V^{-1}\ s^{-1}$. *Nat. Mater.* 9:482–84
92. Allen SJ, Jalan B, Lee S, Ouellette DG, Khalsa G, et al. 2013. Conduction-band edge and Shubnikov–de Haas effect in low-electron-density $SrTiO_3$. *Phys. Rev. B* 88:045114
93. Cain TA, Kajdos AP, Stemmer S. 2013. La-doped $SrTiO_3$ films with large cryogenic thermoelectric power factors. *Appl. Phys. Lett.* 102:182101
94. Keeble DJ, Jalan B, Ravelli L, Egger W, Kanda G, Stemmer S. 2011. Suppression of vacancy defects in epitaxial La-doped $SrTiO_3$ films. *Appl. Phys. Lett.* 99:232905
95. Jalan B, Allen SJ, Beltz GE, Moetakef P, Stemmer S. 2011. Enhancing the electron mobility of $SrTiO_3$ with strain. *Appl. Phys. Lett.* 98:132102
96. Biscaras J, Bergeal N, Kushwaha A, Wolf T, Rastogi A, et al. 2010. Two-dimensional superconductivity at a Mott insulator/band insulator interface $LaTiO_3/SrTiO_3$. *Nat. Commun.* 1:89
97. Annadi A, Putra A, Srivastava A, Wang X, Huang Z, et al. 2012. Evolution of variable range hopping in strongly localized two dimensional electron gas at $NdAlO_3/SrTiO_3$ (100) heterointerfaces. *Appl. Phys. Lett.* 101:231604
98. Chen YZ, Bovet N, Trier F, Christensen DV, Qu FM, et al. 2013. A high-mobility two-dimensional electron gas at the spinel/perovskite interface of γ-$Al_2O_3/SrTiO_3$. *Nat. Commun.* 4:1371
99. Mattheis LF. 1972. Energy bands for $KNiF_3$, $SrTiO_3$, $KMoO_3$, and $KTaO_3$. *Phys. Rev. B* 6:4718–40
100. Mattheiss LF. 1972. Effect of the 110°K phase transition on the $SrTiO_3$ conduction bands. *Phys. Rev. B* 6:4740–53
101. Tsuda K, Tanaka M. 1995. Refinement of crystal structure parameters using convergent-beam electron diffraction: the low-temperature phase of $SrTiO_3$. *Acta Crystallogr. A* 51:7–19
102. Uwe H, Sakudo T, Yamaguchi H. 1985. Interband electronic Raman scattering in $SrTiO_3$. *Jpn. J. Appl. Phys.* 24(Suppl. 24-2):519–21
103. Uwe H, Yoshizaki R, Sakudo T, Izumi A, Uzumaki T. 1985. Conduction band structure of $SrTiO_3$. *Jpn. J. Appl. Phys.* 24(Suppl. 24-2):335–37
104. Janotti A, Steiauf D, Van de Walle CG. 2011. Strain effects on the electronic structure of $SrTiO_3$: toward high electron mobilities. *Phys. Rev. B* 84:201304
105. van Mechelen JLM, van der Marel D, Grimaldi C, Kuzmenko AB, Armitage NP, et al. 2008. Electron-phonon interaction and charge carrier mass enhancement in $SrTiO_3$. *Phys. Rev. Lett.* 100:226403
106. Stern F. 1972. Self-consistent results for *n*-type Si inversion layers. *Phys. Rev. B* 5:4891–99
107. Thiel S, Hammerl G, Schmehl A, Schneider CW, Mannhart J. 2006. Tunable quasi-two-dimensional electron gases in oxide heterostructures. *Science* 313:1942–45
108. Rakhmilevitch D, Neder I, Ben Shalom M, Tsukernik A, Karpovski M, et al. 2013. Anomalous response to gate voltage application in mesoscopic $LaAlO_3/SrTiO_3$ devices. *Phys. Rev. B* 87:125409

109. Bell C, Harashima S, Kozuka Y, Kim M, Kim BG, et al. 2009. Dominant mobility modulation by the electric field effect at the $LaAlO_3/SrTiO_3$ interface. *Phys. Rev. Lett.* 103:226802
110. Caviglia AD, Gariglio S, Reyren N, Jaccard D, Schneider T, et al. 2008. Electric field control of the $LaAlO_3/SrTiO_3$ interface ground state. *Nature* 456:624–27
111. Boucherit M, Shoron OF, Cain TA, Jackson CA, Stemmer S, Rajan S. 2013. Extreme charge density $SrTiO_3/GdTiO_3$ heterostructure field effect transistors. *Appl. Phys. Lett.* 102:242909
112. Altarelli M, Ekenberg U, Fasolino A. 1985. Calculations of hole subbands in semiconductor quantum wells and superlattices. *Phys. Rev. B* 32:5138–43
113. Broido DA, Sham LJ. 1985. Effective masses of holes at GaAs-AlGaAs heterojunctions. *Phys. Rev. B* 31:888–92
114. Neville RC, Hoeneisen B, Mead CA. 1972. Permittivity of strontium titanate. *J. Appl. Phys.* 43:2124–31
115. Khalsa G, MacDonald AH. 2012. Theory of the $SrTiO_3$ surface state two-dimensional electron gas. *Phys. Rev. B* 86:125121
116. Park SY, Millis AJ. 2013. Charge density distribution and optical response of the $LaAlO_3/SrTiO_3$ interface. *Phys. Rev. B* 87:205145
117. Popovic ZS, Satpathy S. 2005. Wedge-shaped potential and Airy-function electron localization in oxide superlattices. *Phys. Rev. Lett.* 94:176805
118. Pentcheva R, Pickett WE. 2007. Correlation-driven charge order at the interface between a Mott and a band insulator. *Phys. Rev. Lett.* 99:016802
119. Son WJ, Cho E, Lee B, Lee J, Han S. 2009. Density and spatial distribution of charge carriers in the intrinsic *n*-type $LaAlO_3$-$SrTiO_3$ interface. *Phys. Rev. B* 79:245411
120. Delugas P, Filippetti A, Fiorentini V, Bilc DI, Fontaine D, Ghosez P. 2011. Spontaneous 2-dimensional carrier confinement at the *n*-type $SrTiO_3/LaAlO_3$ interface. *Phys. Rev. Lett.* 106:166807
121. Khalsa G, Lee B, MacDonald AH. 2013. Theory of t_{2g} electron-gas Rashba interactions. *Phys. Rev. B* 88:041302(R)
122. Zhong ZC, Toth A, Held K. 2013. Theory of spin-orbit coupling at $LaAlO_3/SrTiO_3$ interfaces and $SrTiO_3$ surfaces. *Phys. Rev. B* 87:161102
123. Zhong ZC, Zhang QF, Held K. 2013. Quantum confinement in perovskite oxide heterostructures: tight binding instead of a nearly free electron picture. *Phys. Rev. B* 88:125401
124. Lechermann F, Boehnke L, Grieger D. 2013. Formation of orbital-selective electron states in $LaTiO_3/SrTiO_3$ superlattices. *Phys. Rev. B* 87:241101
125. Chen HH, Kolpak A, Ismail-Beigi S. 2010. First-principles study of electronic reconstructions of $LaAlO_3/SrTiO_3$ heterointerfaces and their variants. *Phys. Rev. B* 82:085430
126. Lee J, Demkov AA. 2008. Charge origin and localization at the *n*-type $SrTiO_3/LaAlO_3$ interface. *Phys. Rev. B* 78:193104
127. Popovic ZS, Satpathy S, Martin RM. 2008. Origin of the two-dimensional electron gas carrier density at the $LaAlO_3$ on $SrTiO_3$ interface. *Phys. Rev. Lett.* 101:256801
128. Santander-Syro AF, Copie O, Kondo T, Fortuna F, Pailhes S, et al. 2011. Two-dimensional electron gas with universal subbands at the surface of $SrTiO_3$. *Nature* 469:189–93
129. Chang YJ, Moreschini L, Bostwick A, Gaines GA, Kim YS, et al. 2013. Layer-by-layer evolution of a two-dimensional electron gas near an oxide interface. *Phys. Rev. Lett.* 111:126401
130. Smoliner J, Berthold G, Strasser G, Gornik E, Weimann G, Schlapp W. 1990. Subband spectroscopy in two-dimensional electron gas systems. *Semicond. Sci. Technol.* 5:308–11
131. Demmerle W, Smoliner J, Berthold G, Gornik E, Weimann G, Schlapp W. 1991. Tunneling spectroscopy in barrier-separated two-dimensional electron-gas systems. *Phys. Rev. B* 44:3090–104
132. Raghavan S, Allen SJ, Stemmer S. 2013. Subband structure of two-dimensional electron gases in $SrTiO_3$. *Appl. Phys. Lett.* 103:212103
133. Hosoda M, Hikita Y, Hwang HY, Bell C. 2013. Transistor operation and mobility enhancement in top-gated $LaAlO_3/SrTiO_3$ heterostructures. *Appl. Phys. Lett.* 103:103507
134. Hirakawa K, Sakaki H, Yoshino J. 1985. Mobility modulation of the two-dimensional electron gas via controlled deformation of the electron wave function in selectively doped AlGaAs-GaAs heterojunctions. *Phys. Rev. Lett.* 54:1279–82

135. Joshua A, Ruhman J, Pecker S, Altman E, Ilani S. 2013. Gate-tunable polarized phase of two-dimensional electrons at the $LaAlO_3/SrTiO_3$ interface. *Proc. Natl. Acad. Sci. USA* 110:9633–38
136. Caviglia AD, Gabay M, Gariglio S, Reyren N, Cancellieri C, Triscone J-M. 2010. Tunable Rashba spin-orbit interaction at oxide interfaces. *Phys. Rev. Lett.* 104:126803
137. Fete A, Gariglio S, Caviglia AD, Triscone J-M, Gabay M. 2012. Rashba induced magnetoconductance oscillations in the $LaAlO_3$-$SrTiO_3$ heterostructure. *Phys. Rev. B* 86:201105(R)
138. Gabay M, Gariglio S, Triscone J-M, Santander-Syro AF. 2013. 2-Dimensional oxide electronic gases: interfaces and surfaces. *Eur. Phys. J.* 222:1177–83
139. Joshua A, Pecker S, Ruhman J, Altman E, Ilani S. 2012. A universal critical density underlying the physics of electrons at the $LaAlO_3/SrTiO_3$ interface. *Nat. Commun.* 3:1129
140. Moetakef P, Ouellette DG, Williams JR, Allen SJ, Balents L, et al. 2012. Quantum oscillations from a two-dimensional electron gas at a Mott/band insulator interface. *Appl. Phys. Lett.* 101:151604
141. Ben Shalom M, Ron A, Palevski A, Dagan Y. 2010. Shubnikov–de Haas oscillations in $SrTiO_3/LaAlO_3$ interface. *Phys. Rev. Lett.* 105:206401
142. Caviglia AD, Gariglio S, Cancellieri C, Sacepe B, Fete A, et al. 2010. Two-dimensional quantum oscillations of the conductance at $LaAlO_3/SrTiO_3$ interfaces. *Phys. Rev. Lett.* 105:236802
143. Huijben M, Koster G, Molegraaf HJA, Kruize MK, Wenderich S, et al. 2010. High mobility interface electron gas by defect scavenging in a modulation doped oxide heterostructure. arXiv:1008.1896v1 [cond-mat.mtrl-sci]
144. Ben Shalom M, Sachs M, Rakhmilevitch D, Palevski A, Dagan Y. 2010. Tuning spin-orbit coupling and superconductivity at the $SrTiO_3/LaAlO_3$ interface: a magnetotransport study. *Phys. Rev. Lett.* 104:126802
145. Fidkowski L, Jiang HC, Lutchyn RM, Nayak C. 2013. Magnetic and superconducting ordering in one-dimensional nanostructures at the $LaAlO_3/SrTiO_3$ interface. *Phys. Rev. B* 87:014436
146. Nakamura H, Koga T, Kimura T. 2012. Experimental evidence of cubic Rashba effect in an inversion-symmetric oxide. *Phys. Rev. Lett.* 108:206601
147. Chen R, Lee S, Balents L. 2013. Dimer Mott insulator in an oxide heterostructure. *Phys. Rev. B* 87:161119(R)
148. Jackson CA, Stemmer S. 2013. Interface-induced magnetism in perovskite quantum wells. *Phys. Rev. B* 88:180403(R)
149. Ouellette DG, Moetakef P, Cain TA, Zhang JY, Stemmer S, et al. 2013. High-density two-dimensional small polaron gas in a delta-doped Mott insulator. *Sci. Rep.* 3:3284
150. Zhang JY, Hwang J, Raghavan S, Stemmer S. 2013. Symmetry lowering in extreme-electron-density perovskite quantum wells. *Phys. Rev. Lett.* 110:256401